Annals of Nuclear Energy, Vol. 5, pp. 569 to 581. Pergamon Press 1978. Printed in Great Britain

ABSOLUTE MEASUREMENTS OF ^{235}U AND ^{239}Pu FISSION CROSS-SECTIONS WITH PHOTONEUTRON SOURCES*

M. C. DAVIS†, G. F. KNOLL, J. C. ROBERTSON and D. M. GILLIAM
The University of Michigan, Ann Arbor

(*Received* 17 *March* 1978)

Abstract—the fission cross-sections of ^{235}U and ^{239}Pu for Na–Be, La–Be, Na–D and Ga–D photoneutrons have been measured absolutely. The neutron source strength was measured using a manganese bath to compare the photoneutron yield from the sources with the standard source NBS-II. Fission counts were accumulated with the source positioned symmetrically between two identical fission foils in an experiment package suspended in a low-albedo laboratory. Fission fragments passing through limited solid angle apertures were recorded on polyester track-etch films. The masses of the foil deposits were determined by microbalance weighings and confirmed by thermal neutron fission and alpha counting. After making a correction for the calculated energy distribution of the source neutrons, values of 1.471 ± 0.029, 1.274 ± 0.026, 1.162 ± 0.025 and 1.195 ± 0.026 barns were obtained for the ^{235}U fission cross-section at the source median energies of 140, 265, 770 and 964 keV, respectively. Corresponding values of 1.469 ± 0.045, 1.515 ± 0.038, 1.670 ± 0.039 and 1.643 ± 0.038 barns were determined for ^{239}Pu.

1. INTRODUCTION

Major facilities for measuring fission cross-sections have been developed in several laboratories. The cross-sections are measured as a function of energy using time-of-flight (TOF) techniques to select the neutron energy. A great deal of information on the shape of the cross-sections versus energy is obtained from a single experiment. However, TOF measurements are usually dependent on knowledge of some standard cross-section. A useful test of the data obtained in this way is provided by measurements using photoneutron sources. These measurements take advantage of the high accuracy obtainable in manganese bath measurements of neutron source strength as discussed by Axton *et al.* (1965). Due to their energy spectra, photoneutron sources are best applied to cross-sections with little or no structure as a function of energy. In the present work, four photoneutron sources were employed to measure absolutely (i.e. independent of any cross-section data) the ^{235}U and ^{239}Pu fission cross-sections at 140, 265, 770 and 964 keV.

* Work supported by Division of Research, USDOE.

† Present address: Department of Engineering Sciences and Applied Mathematics, Northwestern University, Evanston, IL 60201, U.S.A.

2. EXPERIMENTAL METHOD

In general, three basic quantities must be determined to establish a reaction cross-section absolutely: (i) the reaction rate, (ii) the average neutron flux and (iii) the number of target nuclei. In the present work, the corresponding quantities actually measured were: (i) the number of fission tracks recorded on polyester films, the geometry of the limited solid angle apertures, and the duration of the exposure; (ii) the photoneutron source emission rate relative to NBS-II (the secondary standard neutron source of the National Bureau of Standards) and the source–target geometry; and (iii) the mass of deposits.

The basic experimental method has been described previously by Gilliam and Knoll (1975). Modifications in that procedure are pointed out below.

2.1. *An overview of the experimental procedure*

The Ga–D, Na–D and La–Be neutron sources made use of interchangeable spherical cores of compacted Ga_2O_3, NaF or La_2O_3 powder sealed in thin aluminum shells. Hemispherical shells of either deuterated polyethylene or beryllium were attached to surround the core. Figure 1 shows the NaF core, the deuterated polyethylene shells, and mold originally used in forming the shells. The fourth neutron source consisted of a compressed NaF core surrounded by

Table 1. Source characteristics

Source	Inner core Dia. (cm)	Outer shell Dia. (cm)	Half-life (hr)	Median energy (keV)	Initial neutron activity (neutron/sec)
Na–Be	3.01	3.60	15.00	964	5×10^7
La–Be	2.38	3.61	40.23	770	2×10^6
Na–D	2.38	3.65	15.00	265	2×10^7
Ga–D	2.38	3.65	13.95	140	6×10^6

a permanent shell of beryllium. With the exception of the pre-assembled Na–Be source, the inner core was separately irradiated to prevent radiation damage to the outer shells in a reactor neutron flux of 10^{12} neutron/cm^2 sec. A summary of source characteristics is found in Table 1.

Uniform activation during the irradiation was assured by continuously rotating the source at the reactor mid-plane to a saturated activity. The source was then remotely transferred to the adjacent hot cave where the photoneutron target shells were added (not necessary for the pre-assembled Na–Be source). The assembled source was transferred to a low-albedo laboratory.

The fission rate measurement and the manganese bath comparisons were carried out in a thick walled concrete cell (Fig. 2) with a mean inside diameter of 4.2 m. All the interior surfaces of the cell are lined with a 5 cm layer of anhydrous borax to reduce the return of moderated neutrons into the experimental area. The manganese bath was drained during the fission rate measurement in order that the full advantage of the borax lining be realized.

At the center of the low-albedo cell, the photoneutron source was positioned symmetrically between two track-etch fission detectors as shown for plutonium measurement in Fig. 3. The source and detectors were supported by a lightweight tubular framework which was enclosed in a cadmium-lined drum 60 cm in diameter. The uranium measurements at 140, 265 and 964 keV were in a helium environment whereas the 770 keV measurement was conducted in vacuum. All plutonium measurements were made in vacuum using a smaller tubular framework inside a 23 cm diameter brass containment cylinder (Fig. 4).

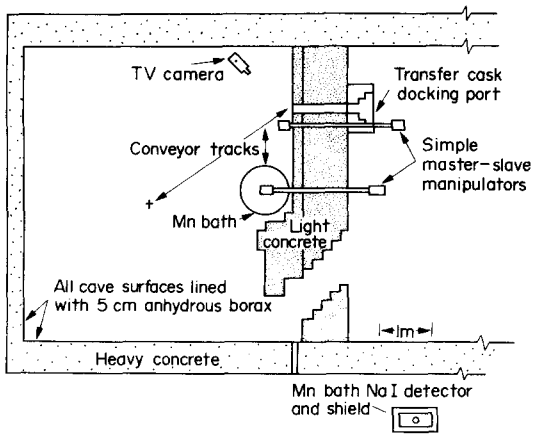

Fig. 2. Floor plan of the photoneutron laboratory.

The total fission rate with the limited solid angle detectors is insensitive to the positioning of the neutron source, so that an accurate measurement of the location of the highly radioactive photoneutron source was not necessary. Instead, a precise measurement was carried out of the target-to-target spacing both before and after the fission rate determination. Each detector supported one or two nearly identical target foils of 1 mg/cm^2 thick, 2.76 cm diameter deposits on 20 mil platinum. The timing of the track accumulation period was defined by placement of the photoneutron source in the detector package source well for the measurements in vacuum, and by electrically activated shutters that interposed between the fissionable deposit and the track-etch film for the helium environment. Two runs were made for each measurement varying the dual foil spacing from 10 cm to 18 cm to permit evaluation of the background due to room-return neutrons.

The polyester track-etch films (Dupont Cronar, 4 mil thickness) were etched in KOH to develop the tracks to an average diameter of about 14 μm. The tracks were counted manually on a projection microscope.

Following the fission rate measurements, the neutron source was transferred to a continuously sampled manganese bath (Fig. 5). Measurements of the standard NBS-II before and after each run served to calibrate the bath efficiency.

The masses of the deposits were determined by the supplier, The Isotope Target Laboratory at Oak Ridge National Laboratory, by means of microbalance weighings. The relative isotopic content was determined by mass spectrographic analysis also per-

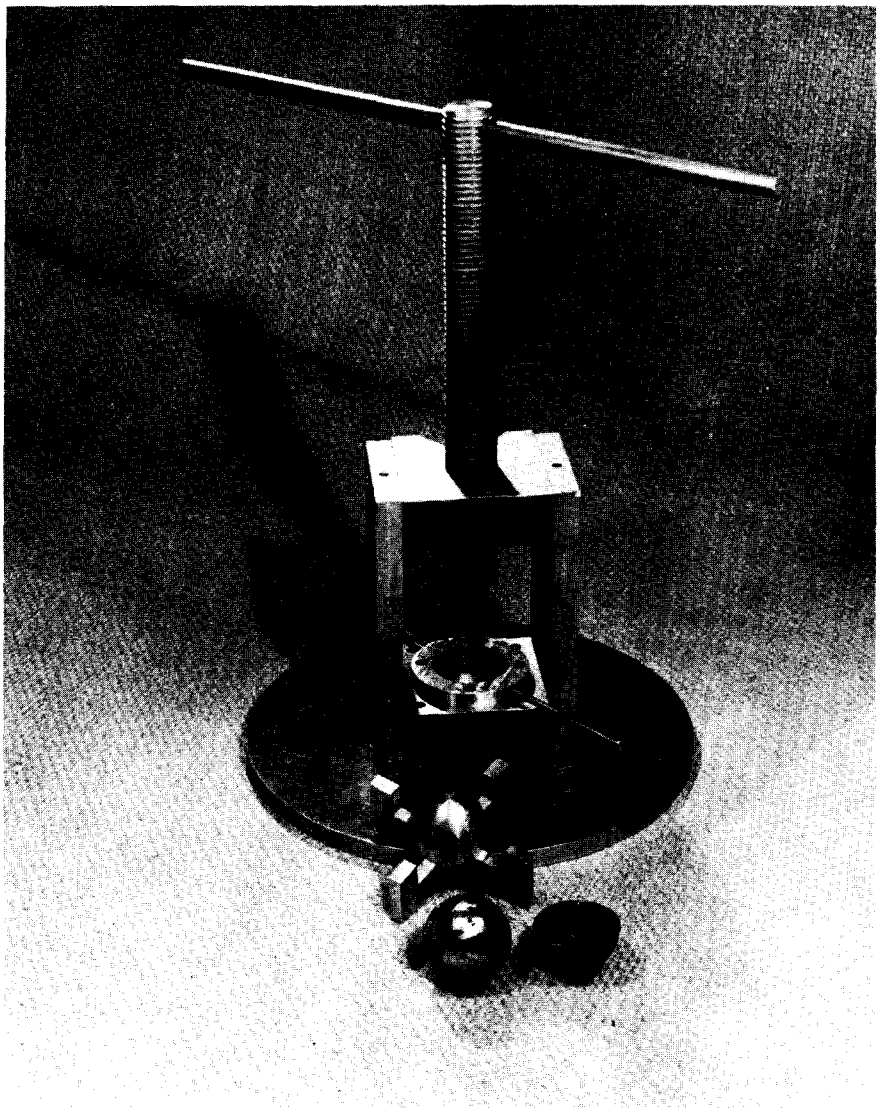

Fig. 1. Deuterated polyethylene shells and gamma-emitting core mold used for fabrication, and press used for 'hot' assembly.

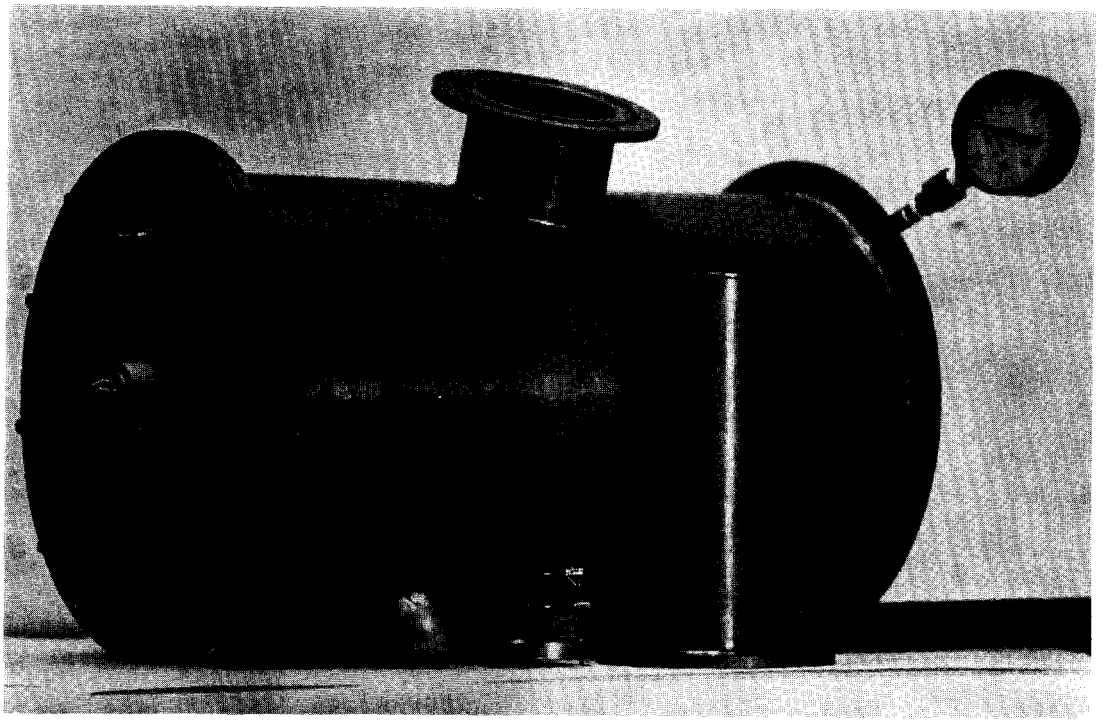

Fig. 4. Plutonium containment package.

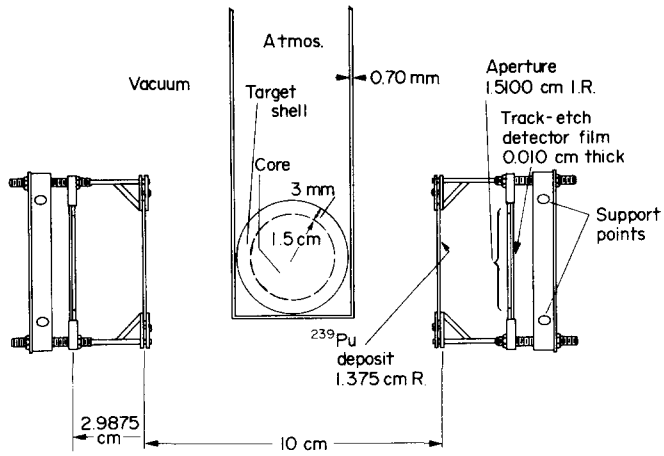

Fig. 3. Plutonium detector and source arrangement.

formed at ORNL. Confirming mass assays by alpha and thermal neutron fission counting were conducted at the National Bureau of Standards.

3. DATA ANALYSIS, CORRECTIONS AND RESIDUAL ERRORS

The cross-section was calculated based on the total number of fissions produced, the mass of the deposits and the neutron flux at the target positions.

3.1. *The average scalar flux*

The average scalar flux was obtained from the measured source strength and source-to-foil geometry measurements. A computer code was developed to unfold the time dependence of the photoneutron exponential decay, ^{56}Mn activation, and the mixing delays in the manganese bath detector system. The photoneutron half-life values and mixing behavior have been sufficiently well determined from prior work (Bowman, 1976; Robertson *et al.*, 1975) so that the adjusted saturated activity values showed no deviation other than statistical variation over the entire 36-hour activation–decay cycle. The weighted average of the saturated activity over the entire cycle had a statistical precision of about 0.03%, and repeated counts with the NBS-II reference source before and after each fission rate measurement showed reproducibility of better than 0.1%. As discussed by Gilliam and Knoll (1975), the source strength of NBS-II was taken as $1.174 \times 10^6\ \text{sec}^{-1} \pm 0.5\%$, referred to June 1972.

Small corrections were applied to the manganese bath results to account for parasitic absorption of neutrons in the source and walls of the dry well, and photoneutron production caused by the natural deuterium content of the aqueous solution. The parasitic neutron absorption in the source and dry well was approximated by the product of the measured thermal flux and the total macroscopic thermal absorption cross-section of all nuclei in the source and dry well. The thermal neutron flux at the source position

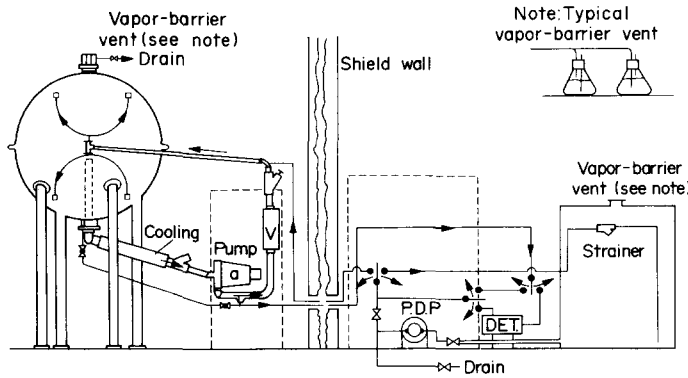

Fig. 5. Continuously sampled manganese bath.

of the dry well was measured by placing $MnSO_4 \cdot H_2O$ absorbers above and below the source. The change in the saturated activity in the bath was proportional to the thermal re-entry flux. No correction was applied for the flux depression, thermal self-shielding or epithermal absorption. These approximations seemed appropriate in view of ANISN calculations showing epithermal absorption at less than 4% of the total absorption in the sources. The magnitude of this correction ranged from (0.59 ± 0.13)% for Na–Be to (0.08 ± 0.15)% for Ga–D. Photoneutron production by the natural deuterium content of the aqueous manganous sulfate solution was determined by comparing the saturated activity produced by the bare gamma-emitting core of the source with the activity from the fully assembled source. This correction was determined to be (0.95 ± 0.10)% for the beryllium sources and (0.72 ± 0.10)% for the deuterium sources. Bulk penetration leakage from the bath was measured using a long counter and found negligible for all sources.

In this experiment the cross-section was derived from the sum of the fluxes at the two deposits and the combined fission rates. The obvious advantage of this method is that it is significantly easier to get an accurate value for the sum of the fluxes on the two deposits than for the individual fluxes. An estimated error in the measurement of the foil spacing, ±0.008 cm for the 10 cm foil separation, led to an uncertainty of 0.16% in the sum of the fluxes, while the estimated error in the source centering, ±0.050 cm, led to an uncertainty of only 0.0028% in the sum of the fluxes.

The angular distribution of neutron emission was taken into account in computing the average scalar flux acting on the fission deposits at the various source–foil spacings. The spherical shell geometry gave rise to a peaked angular distribution at angles of maximum chord length through the shell. At a source–foil spacing of 5 cm, the off-radial peaking resulted in a scalar flux of about 3% higher intensity than would have been realized from a point source of the same emission rate at the same spacing. Offsetting influences of the finite size of the deposit surface and of the source resulted in only a small departure from a point-source, point-target approximation to the average scalar flux at the deposit surface. This behavior is shown as a function of source–foil spacing in Fig. 6.

The measured non-uniform uranium distribution on the deposits was taken into account in computing its weighted average scalar flux over the target nuclei on the two deposits.

Corrections of the order of 2–5% were calculated

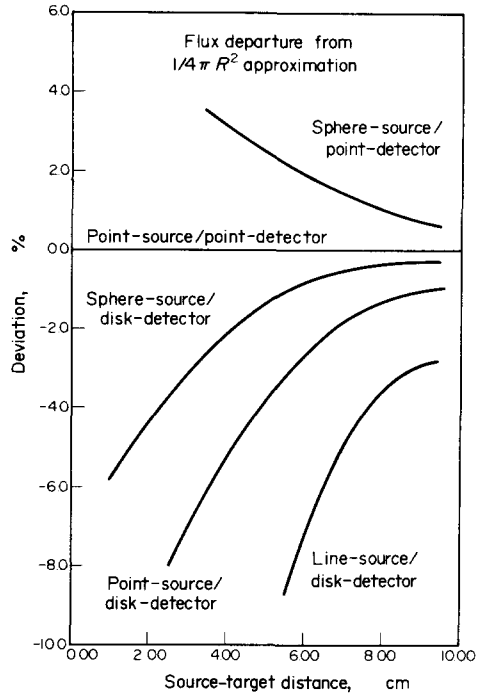

Fig. 6. Flux per unit source strength departures from point-source/point-detector approximation.

for scattering from the platinum backing, supporting apparatus, and containment vessel. Scattering in the backings was calculated by means of a Monte-Carlo program, taking into account the anisotropy of scattering in platinum. In-scatter to the deposit at angles near the deposit plane was found to override out-scatter so that the net effect was to increase the scalar flux. This correction varied from (1.67 ± 0.21)% for Na–Be to (3.07 ± 0.38)% for Ga–D. This calculation was partially verified by an experiment in a thermal neutron beam by increasing the backing thickness and measuring the increase in scattering. Of lesser magnitude was the correction for scattering in the support structure (0.3–0.5%) and in the vacuum containment vessel (0.6–1.0%).

3.2. *Mass of the deposits*

The masses of the U_3O_8 deposits were determined to be 8.16 mg and 6.85 mg by microbalance weighings in an inert atmosphere at regulated pressure. Workers in the Isotope Target Laboratory at ORNL estimate that these weighings were accurate to ±2 μg. However, for the reasons discussed in Gilliam and Knoll (1975), a more conservative accuracy of ±30 μg has been assumed.

The plutonium deposits were alpha counted relative to the NBS foil standard, 49K-4-1, whose isotopic composition was identical to the foils used in these

measurements. Masses of 5.59 mg and 4.94 mg were determined. The 1.4% accuracy in the PuO_2 mass was dominated by a 1.2% uncertainty in the reference foil mass.

A correction to account for the isotopic fission contribution to the total fission rate was less than 0.15% and 0.02% for the uranium and plutonium cross-sections respectively.

3.3. *The total number of fissions produced in the deposits*

The total number of fission events was obtained from the track counts and the calculated detector efficiency.

In addition to the imprecision always associated with Poisson distributed counts, an uncertainty of 0.5% due to scanner bias was assumed based on the average difference in repeated counts of the samples by different scanners. This reproducibility error resulted primarily from judgment inconsistencies in applying the shape, size, and depth criteria for track acceptance in borderline cases. Unresolvable coincidences in the track locations required a very small correction and associated uncertainty (0.24% or less on any single film). No uncertainty was associated with the discrimination against alpha and background pits. The largest alpha track diameters observed never exceeded 7 μm whereas the smallest fragment was greater than 10 μm. A registration efficiency of $100 \pm 0\%$ has been assumed for the track-etch method of fission counting using limited solid angle counting on the basis of tests reported by Gilliam and Knoll (1970).

By means of an arrangement of gauge blocks and 0.00005 in. dial indicators, reproducibilities of better than 0.0008 cm (0.0003 in.) were obtained in repeated measurements of the deposit–aperture spacing. An uncertainty of 0.0025 cm was assumed in this spacing, however, because of deviations from perfectly flat, parallel geometry. The aperture diameter was determined within ± 0.002 cm by means of a metallurgical microscope with 0.0001 in. stage micrometers.

A computer code to calculate the efficiency of detection was written with provisions for including the significant anisotropy of fragment emission, the measured uranium thickness distribution, and the computer scalar flux variation over the deposit area. Table 2 summarizes our anisotropy evaluation based on the available data for the empirical fitting function $W(\theta) = 1 + A\cos^2\theta$, where θ is the angle in the laboratory coordinates. The column headed 'ΔA' lists estimated uncertainties in the anisotropy factor, and the '$\Delta\sigma$' column shows the corresponding uncertainties in the cross-section which result. Independent measurements by Hsue (1976) of the anisotropy factor at each of the source energies using similar track-etch techniques were weighted together with these measurements of Caruana *et al.* (1974), Smirenkin *et al.* (1970), Huizenga and Behkami (1968), Nesterov *et al.* (1967) and Simmons and Henkel (1960). The estimate of the error in this adjustment was taken to be standard deviation of the variance in the available data. The computed efficiency was as high as $(5.79 \pm 1.36)\%$ higher for ^{239}Pu at 964 keV than the corresponding value for isotropic emission. Gilliam and Knoll (1975) originally relied on the Nesterov data only to derive the ^{235}U fission cross-section at 964 keV. The correct normalization of the $W(\theta)$ function must account for the momentum of the compound nucleus and the slight subsequent forward bias in the angular distribution. The emission into the forward 2π solid angle for incident 964 keV neutrons was found to be 1.0049 ± 0.0012 fragment per fission by means of a simple kinematics calculation based on average fragment mass values. The uncertainties in the measurements of the aperture diameter and deposit–aperture spacing led to residual errors in the detector efficiency of only $\pm 0.13\%$ and $\pm 0.14\%$, respectively. The non-uniformity of the uranium oxide thickness and the neutron flux variation over the target area were found to have only small influence on the detector efficiency, resulting in insignificant residual errors.

3.4. *Spectrum-averaged cross-section and the normalization to point energy values*

The reaction rate measured led directly to the spectrum-average cross-section value

$$\sigma_f = \int_E \Theta(E)\sigma_f(E)\mathrm{d}E \Big/ \int_E \Theta(E)\mathrm{d}E.$$

Table 2. Evaluated fission fragment emission anisotropy

Source	E_n(keV)	^{235}U		^{239}Pu	
		$A + \Delta A$	$\Delta\sigma$	$A + \Delta A$	$\Delta\sigma$
Na–Be	964	0.158 ± 0.030	∓ 1.168	0.116 ± 0.030	∓ 1.362
La–Be	770	0.111 ± 0.030	∓ 1.034	0.117 ± 0.030	∓ 0.934
Na–D	265	0.030 ± 0.030	∓ 1.374	0.109 ± 0.030	∓ 1.372
Ga–D	140	0.007 ± 0.030	∓ 1.123	0.080 ± 0.030	∓ 1.418

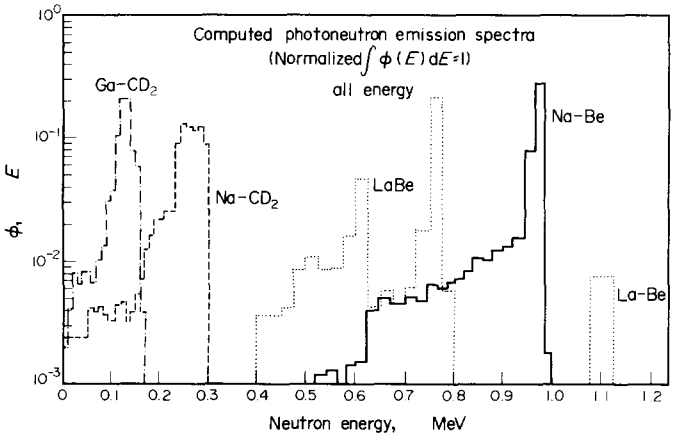

Fig. 7. Photoneutron energy spectra.

A correction was made to account for the cross-section variation over the photoneutron energy spectrum and to adjust the spectrum-averaged result to the median energy of the spectrum. The energy spectrum was computed from a Monte-Carlo code which adapted subroutines from a similar code by Bensch and Vesely (1969). The computed spectra are shown in Fig. 7. The tail of neutrons of degraded energy is produced by neutron scattering and gamma (Compton) scattering within the source. The complex La–Be spectrum is due to the multiple gamma lines above the beryllium (γ, n) threshold. The energy correction factors are listed in Table 3. The ENDF/B and Sowerby evaluated data sets were used to estimate the uncertainty due to fission cross-section shape. Since this shape is slowly varying over the photoneutron energy range for both ^{235}U and ^{239}Pu, this correction was for most cases less than $1(\pm 0.3)\%$. The exceptions were the lower energy points, 140 and 265 keV, for ^{235}U where a steeper negative slope (see Fig. 10) in the fission cross-section resulted in an adjustment as large as 3%.

The total neutron flux at the deposit is the sum of the direct streaming from the source and of the room-scattered flux. The room-scattered flux is proportional to the source strength just as is the direct flux. In a large room with the source at the center, the room-scattered flux is very nearly constant over small displacements in the neighbourhood of the source, while the direct streaming drops off approximately as $1/R^2$, where R is the source-to-target distance. The qualification 'approximately' must be included because of the angular distribution of the source emission and the finite extent of the fission deposit. Figures 8 and 9 are plots of the apparent

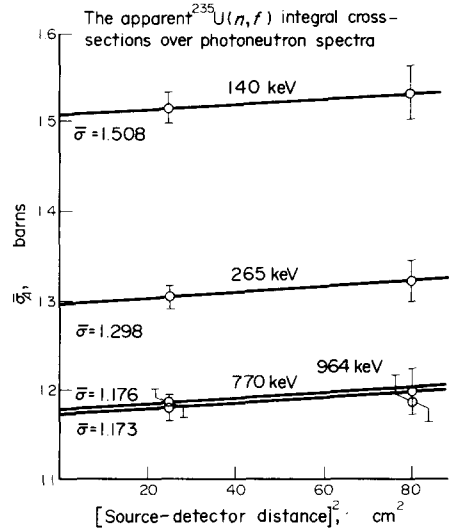

Fig. 8. The apparent ^{235}U(n,f) integral cross-sections over photoneutron spectra vs R^2_{cm}.

Table 3. Photoneutron energy spectrum corrections

E_n (keV)	^{235}U ENDF/B-IV	^{235}U ENDF/B-V	^{235}U Sowerby	^{239}Pu ENDF/B-IV	^{239}Pu Sowerby
964	1.00899	1.01598	1.01089	1.00573	1.01044
770	0.98438	0.98593	0.99129	1.01810	1.01514
265	0.97426	0.97135	0.97782	0.99786	0.99941
140	0.96878	0.94883	0.97033	0.99107	0.98642

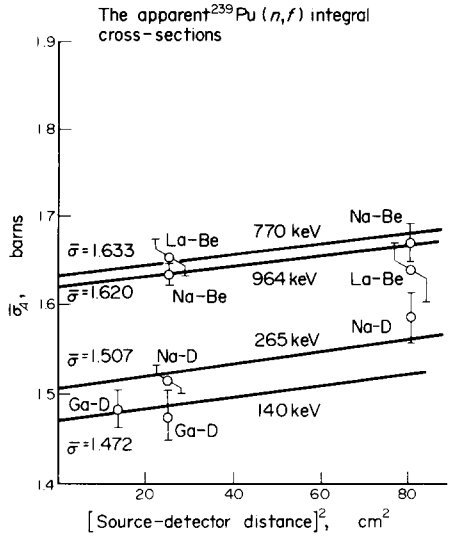

Fig. 9. The apparent $^{239}Pu(n,f)$ integral cross-sections vs R^2_{eff}.

cross-section values as a function of R^2. The room-scatter contribution was assumed equal for all uranium and plutonium measurements where the same support structure was utilized. The assumption appeared valid in view of the collective experimental results and ANISN calculations showing the room-scattered flux virtually independent of both the source energy and position. The room-scattered contribution to the total fission rate (the slope in Figs 8 and 9) was experimentally determined to be $(0.03 \pm 0.01)\%$ cm^{-2}.

Tables 4 and 5 summarize the corrections applied to this measurement. The sign attached to each correction is the sign of the associated change in the cross-section value due to the particular adjustments cited. The changes affect the final cross-section value nearly in the proportion cited.

Tables 6 and 7 summarize the uncertainties in the ^{235}U (n,f) and ^{239}Pu (n,f) cross-section measurements, respectively. The common error-propagation

Table 4. Adjustments and corrections with residual errors for ^{235}U

Type of perturbation	Resulting correction (%) Na–Be	La–Be	Na–D	Ga–D
Fragment emission anisotropy*	−6.65 ± 1.17	−4.11 ± 1.03	−1.42 ± 1.37	−0.27 ± 1.12
Angular distribution normalization to lab	−0.49 ± 0.12	−0.44 ± 0.11	−0.26 ± 0.06	−0.19 ± 0.05
D(γ,n) reaction in solution	+0.94 ± 0.10	+0.96 ± 0.10	+0.72 ± 0.10	+0.72 ± 0.10
Parasitic absorption	+0.41 ± 0.10	+0.17 ± 0.15	+0.27 ± 0.14	+0.08 ± 0.15
Leakage	0.0 ± 0.05	0.0 ± 0.05	0.0 ± 0.05	0.0 ± 0.05
Scattering in Pt backings	−1.67 ± 0.21	−1.62 ± 0.20	−2.59 ± 0.18	−3.07 ± 0.38
Scattering in other structures	−0.33 ± 0.17	−0.38 ± 0.19	−0.36 ± 0.18	−0.47 ± 0.24
Foil impurities	−0.15 ± 0.04	−0.06 ± 0.02	0.00 ± 0.02	0.00 ± 0.02
Energy spectrum	+0.90 ± 0.30	−1.56 ± 0.30	−2.57 ± 0.30	−3.12 ± 0.30

* Note: Correction is already included in the solid angle efficiency calculations.

Table 5. Adjustment and corrections with residual errors for ^{239}Pu

Type of perturbation	Resulting correction (%) Na–Be	La–Be	Na–D	Ga–D
Fragment emission anisotropy	−5.79 ± 1.36	−3.93 ± 0.93	−5.45 ± 1.37	−4.05 ± 1.42
Angular distribution normalization to lab	−0.49 ± 0.12	−0.44 ± 0.11	−0.26 ± 0.06	−0.19 ± 0.05
D(γ,n) reaction in solution	+0.94 ± 0.10	+0.96 ± 0.10	+0.72 ± 0.10	+0.72 ± 0.10
Parasitic absorption	+0.41 ± 0.13	+0.17 ± 0.15	+0.27 ± 0.14	+0.80 ± 0.15
Leakage	0.0 ± 0.05	0.0 ± 0.05	0.00 ± 0.05	0.00 ± 0.05
Scattering in Pt backings	−1.67 ± 0.21	−1.62 ± 0.20	−2.59 ± 0.32	−3.07 ± 0.38
Scattering in foil holder	−0.31 ± 0.05	−0.58 ± 0.10	−0.41 ± 0.07	−1.09 ± 0.19
Scattering in other structures	−0.84 ± 0.19	−0.92 ± 0.21	−1.21 ± 0.32	−1.13 ± 0.28
Foil impurities	−0.02 ± 0.04	−0.01 ± 0.04	0.00 ± 0.04	−0.00 ± 0.04
Energy spectrum	+0.57 ± 0.30	+1.81 ± 0.30	−0.21 ± 0.30	−0.89 ± 0.30

Table 6. Summary of major uncertainties in ^{235}U measurements

Experimental factor	Resulting uncertainty (%) Na–Be	La–Be	Na–D	Ga–D
Propagated error in net fission cts/source neutron	1.39	1.51	1.00	1.18
Manganese bath comparison of sources	0.25	0.26	0.25	0.26
Fragment emission anisotropy	1.17	1.03	1.37	1.12
Angular distribution normalization to lab	0.12	0.11	0.06	0.05
Half-life extrapolation	0.57	0.25	0.25	0.25
NBS-II reference source	0.50	0.50	0.50	0.50
^{235}U foil masses	0.50	0.50	0.50	0.50
Scattering in Pt backings	0.21	0.20	0.32	0.38
Scattering in other structures	0.17	0.19	0.18	0.24
Propagated errors in compensated beam geometry	0.57	0.57	0.57	0.57
Energy spectrum	0.30	0.30	0.30	0.30
Total random error	1.51	1.62	1.17	1.33
Total systematic error	1.55	1.35	1.64	1.47
Quadrature sum	2.16	2.11	2.01	1.98

formula,

$$\sigma_f^2(x, y, \ldots) = \left(\frac{df}{dx}\right)^2 \sigma_x^2 + \left(\frac{df}{dx}\right)^2 \sigma_y^2 + \cdots$$

was used to combine the independent uncertainties. All error sources were treated as symmetric, whereas some error components were actually asymmetric. All estimated errors were to be interpreted as one stan-

Table 7. Summary of major uncertainties in ^{239}Pu measurements

Experimental factor	Resulting uncertainty (%) Na–Be	La–Be	Na–D	Ga–D
Propagated error in net fission cts/source neutron	0.81	1.34	1.20	2.07
Manganese bath comparison of sources	0.25	0.26	0.25	0.26
Fragment emission anisotropy	1.36	0.93	1.37	1.42
Angular distribution normalization to lab	0.12	0.11	0.06	0.05
Half-life extrapolation	0.25	0.25	0.25	0.25
NBS-II reference source	0.50	0.50	0.50	0.50
^{239}Pu foil masses	1.40	1.40	1.40	1.40
Scattering in Pt backings	0.21	0.20	0.32	0.38
Scattering in other structures	0.20	0.23	0.33	0.34
Propagated errors in compensated beam geometry	0.57	0.57	0.57	0.57
Energy spectrum	0.30	0.30	0.30	0.30
Total random error	1.01	1.47	1.34	2.15
Total systematic error	2.08	1.83	2.12	2.16
Quadrature sum	2.32	2.35	2.51	3.05

Table 8. Final cross-section values and estimated residual errors

Neutron source energy (keV)	$^{25}\sigma_f(n,f)$	$^{49}\sigma_f(n,f)$	$^{49}\sigma_f(n,f)/^{25}\sigma_f(n,f)$
140	1.471 ± 0.029	1.469 ± 0.045	0.999 ± 0.035
265	1.274 ± 0.026	1.515 ± 0.038	1.189 ± 0.037
770	1.162 ± 0.025	1.670 ± 0.039	1.437 ± 0.044
964	1.195 ± 0.026	1.643 ± 0.038	1.375 ± 0.041

dard deviation. Random errors included statistics in fission counting and manganese-bath comparison, and uncertainties in the source–foil–aperture geometry. All remaining sources of error were treated as systematic. Experimental conditions were not ideal for deriving cross-section ratios; however, many errors associated with source yield and energy spectrum did cancel resulting in a final uncertainty in the ratios less than the quadrature sum of the individual absolute measurements.

Table 8 lists the final cross-section values and estimated residual errors. The change in the value at 964 keV for ^{235}U from that previously reported (Gilliam and Knoll, 1975) reflects the current evaluation of the fission fragment anisotropy data at that energy.

4. DISCUSSION

4.1. ^{235}U (n, f) *cross-section*

These results for ^{235}U (n,f) cross-section are compared to other experimental work and evaluations in Fig. 10. There appears to be good consistency in the data at the extreme points; Poenitz (1974), White (1965), Barton *et al.* (1976), Czirr and Sidhu (1975) and this work agree very well at approximately 1 MeV; and at 140 keV, Szabo *et al.* (1970, 1971, 1973), Poentiz (1974), Khuravlev *et al.* (1976) and the new data agree. However, between 200 and 700 keV, there appears a shape discrepancy between various evaluations. The 265 keV point lies between the two ENDF/B evaluations and in reasonable agreement with Szabo and Poentiz, but higher than the Wasson (1976) data and the Czirr data. The 770 keV value is clearly higher than most, but in the company of Kappeler (1971) and again Szabo. In general, the measurements all agree within ±3% of the ENDF/B-IV values.

4.2. ^{239}Pu (n, f) *cross-section*

There are relatively few direct measurements on the ^{239}Pu (n,f) cross-section and even fewer absolute measurements (reference Fig. 11). Szabo employed several methods of absolute flux determinations, including the manganese bath calibration and the associated flux particle method. ^{239}Pu measurements are relative to his absolute ^{235}U (n,f) measurements. The data of Allen and Fergenson (1957) includes an absolute measurement at 550 keV and 1.5 MeV. The scatter and the sparseness in the data presented is due to the difficulty of direct ^{239}Pu measurements and the relative ease of ratio measurements.

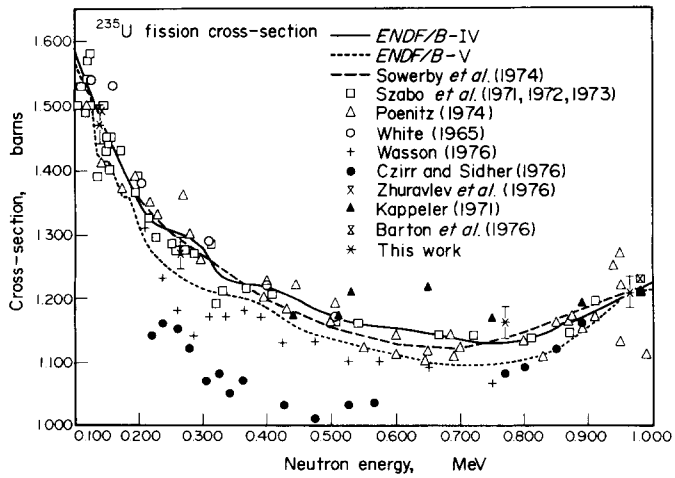

Fig. 10. $^{235}U(n,f)$ cross-section between 0.1 and 1.0 MeV.

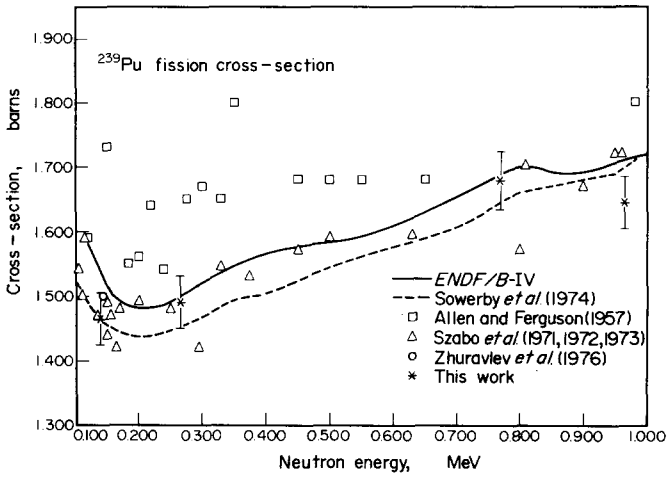

Fig. 11. $^{239}Pu(n,f)$ cross-section between 0.1 and 1.0 MeV.

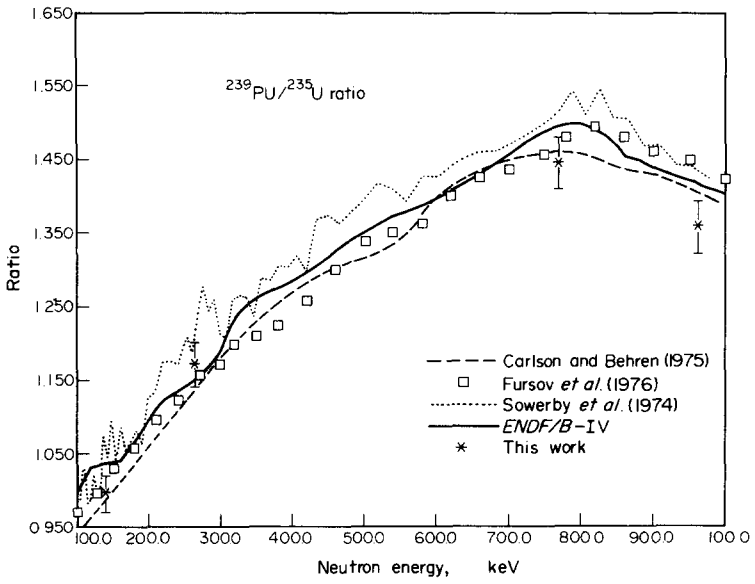

Fig. 12. 49/25 Ratio between 0.1 and 1.0 MeV.

4.3. $^{239}Pu/^{235}U$ *ratio*

Figure 12 compares the present work to the data of Carlson and Behrens (1975) and Fursov *et al.* (1975). Agreement is within the error associated with the evaluations for this energy interval.

Acknowledgements—The authors wish to acknowledge W. P. Stepany, J. C. Engdahl and D. T. Grady for their contributions during various stages of the experimental work. Analysis and counting of fission tracks were carried out by K. Fleming, L. Grady, G. Lovett, D. Schoen and S. Slezak, for which we are grateful.

REFERENCES

Allen W. D. and Ferguson A. T. G. (1957) *Proc. phys. Soc.* **A70,** 573.

Axton E. J., Cross P. and Robertson J. C. (1965) *J. nucl. Energy* A/B **19,** 409.

Barton D. M., Diven B. C., Hansen G. E., Jarvis G. A., Koohtz P. G. and Smith R. K. (1976) *Nucl. Sci. Engng* **60,** 369.

Bensch F. and Vesely F. (1969) *J. nucl. Energy* A/B **23,** 537.

Bowman W. C. (1976) Master's Dissertation, University of Michigan.

Carlson C. W. and Behren's J. W. (1975) USERDA, Report *UCID*-16981, Lawrence Livermore Laboratory.

Caruana J., Mathus J. N., Boldeman J. W. and Walsh R. L. (1974) *Proc. Indian Nucl. Phys. Solid State Phys. Sym.*, Trombay, 1974.
Czirr J. B. and Sidher G. S. (1976) *Nucl. Sci. Engng* **60**, 383.
Fursov B. I., Kuprisanov V. and Smirenkin G. (1976) *IAEA Panel on Neutron Standards and Reference Data*, Vienna (to be published).
Gilliam D. M. and Knoll G. F. (1970) *Trans. Am. nucl. Soc.* **13**, 526.
Gilliam D. M. and Knoll G. F. (1975) *Ann. nucl. Energy* **2**, 637.
Hsue S. T. (1976) Master's Dissertation, University of Michigan.
Huizenga J. R. and Behkami A. N. (1968) *Phys. Rev.* **174**, 1539.
Kappeler F. (1971) *Neutron Standards and Flux Normalization*. AEC Symposium Series 23, Argonne 1970, p. 272.
Nesterov V. G., Smirenkin G. N. and Shpak D. L. (1966) *Yad. Fiz.* **4**, 933.
Poenitz W. P. (1974) *Nucl. Sci. Engng* **53**, 370.
Robertson J. C., Davis M. C. and Engdahl J. C. (1975) *Conf. on Neutron Cross Sections and Technology*, Washington D.C., NBS SP 425, 112.
Simmons J. E. and Henkel R. L. (1960) *Phys. Rev.* **120**, 198.
Smirenkin G. N., Shpak D. L., Ostapenko Y. B. and Fursov B. I. (1970) *J. exp. theor. Phys. Lett.* **11**, 333.
Sowerby M. C., Patrick B. H. and Mather D. S. (1974) *Ann. nucl. Sci. Engng* **1**, 409.
Szabo I., Fillippi G., Huet J. L., Leroy J. L. and Marquette J. P. (1971) *Neutron Standards and Flux Normalization*, AEC Symposium Series 23, Argonne, 1970, p. 257.
Szabo I., Leroy J. L. and Marquette J. P. (1972) *IAEA Panel on Neutron Standards and Reference Data*, Vienna.
Szabo I., Leroy J. L. and Marquette V. P. (1973) *Conf. on Neutron Physics*, Kiev, 1973, Vol. 3, p. 27.
Wasson O. A. (1976) *Proc. NEANDC/NEACRP Spec. Meeting on Fast Neutron Fission Cross Sections*, Argonne, 1976, p. 183.
White P. H. (1965) *J. nucl. Energy* A/B **19**, 325.
Zhuravlev K. D., Kroshkin N. I. and Karin L. V. (1976) *Int. Conf. on the Interactions of Neutrons with Nuclei*, Lowell, 1976 (to be published).